

A MONTE-CARLO CODE FOR THE DETAILED SIMULATION OF ELECTRON AND LIGHT-ION TRACKS IN CONDENSED MATTER

D. Emfietzoglou^{1,6}, G. Papamichael², K. Karava¹, I. Androulidakis³, A. Pathak⁵, G. W. Phillips⁶, M. Moscovitch⁶ and K. Kostarelos^{4,*}

¹Department of Medical Physics, University of Ioannina Medical School, Ioannina 451 10, Greece

²Department of Mechanical Engineering, National Technical University of Athens, Athens 157 10, Greece

³Department of Physics, University of Ioannina, Ioannina 451 10, Greece

⁴The School of Pharmacy, University of London, London WC1N 1AX, UK

⁵School of Physics, University of Hyderabad, Hyderabad 500 046, India

⁶Department of Radiation Medicine, Georgetown University Medical Center, Washington DC 20007, USA

In an effort to understand the basic mechanism of the action of charged particles in solid radiation dosimeters, we extend our Monte-Carlo code (MC4) to condensed media (liquids/solids) and present new track-structure calculations for electrons and protons. Modeling the energy dissipation process is based on a model dielectric function, which accounts in a semi-empirical and self-consistent way for condensed-phase effects which are computationally intractable. Importantly, these effects mostly influence track-structure characteristics at the nanometer scale, which is the focus of radiation action models. Since the event-by-event scheme for electron transport is impractical above several kilo-electron volts, a condensed-history random-walk scheme has been implemented to transport the energetic delta rays produced by energetic ions. Based on the above developments, new track-structure calculations are presented for two representative dosimetric materials, namely, liquid water and silicon. Results include radial dose distributions in cylindrical and spherical geometries, as well as, clustering distributions, which, among other things, are important in predicting irreparable damage in biological systems and prompt electric-fields in microelectronics.

INTRODUCTION

Monte-Carlo (MC) simulation has become an important tool for studying radiation action in both living and non-living systems. The reason being that radiation effects are often associated with functional alterations at the micrometer–nanometer scale where direct experimental information is difficult to obtain. For example, stochastic distributions and clustering properties of single-tracks are best obtained by computational means. Such knowledge is important for assessing the quality of the beam and for analysing the so-called LET-dependence response of a system (e.g. solid detectors or biological cells)⁽¹⁾.

The above information is difficult to obtain by the general-purpose MC codes (e.g. MCNP, EGS/BEAM, GEANT, ITS, FLUKA, PENELOPE) which adopt an effective electron energy cut-off (>0.1–1 keV) and an artificial transport-step. A fully microscopic, event-by-event, scheme presents a challenge in terms of low-energy electron interaction physics, since the details of the electronic structure of the target become critical at this range⁽²⁾. In that respect, it is important to account for distinctive

features of condensed media relative to gases, such as⁽³⁾ (1) the long-range polarisation of the material and screening of the projectile's field, which leads to weaker scattering probabilities, especially at low incident energies; (2) the collective transitions because of the large electronic density, which results in stronger absorption probabilities at certain energy losses and (3) the lower ionisation thresholds because of quasi-free electron states in the conduction band and the general shifting of the absorption spectrum to higher losses, which lead to a higher ionisation efficiency. Importantly, these effects influence track-structure characteristics in the nanometer scale (1–100 nm).

The energy loss mechanisms included in the MC4 version for condensed media may be classified as follows: (1) incoherent transitions leading to ionisations in the liquid and electron–hole production in the solid, (2) single-particle coherent transitions leading to discrete excitations in the liquid (excitons in solids are not included) and (3) many-particle coherent transitions leading to plasmon excitations in the solid. Although a semi-classical theory may be used for core-electrons (i.e. K-shell), the use of a model dielectric function approximation is the method of choice for the valence-electrons, since it allows in a semi-empirical and self-consistent way for the inclusion of condensed-phase effects. It has

*Corresponding author: kostas.kostarelos@pharmacy.ac.uk

been extensively used by the Oak Ridge⁽⁴⁾ and NIST⁽⁵⁾ groups, as well as by others⁽⁶⁻⁹⁾ while the method of the Barcelona group^(10,11) (implemented in PENELOPE and LEEPS) may be considered as an equivalent formulation. More recently, the dielectric approximation has been implemented in the code PARTRAC⁽¹²⁾ and the code by Cobut *et al.*⁽¹³⁾, while our group has provided a detailed analysis of its application to electron and proton transport in condensed media⁽¹⁴⁻¹⁹⁾. An *ab initio* calculation of the dielectric function has also been implemented in the Columbia code⁽²⁰⁾. In the following paper, a summary of the dielectric approximation as used in MC4 for condensed matter is presented, along with some typical microscopic calculations for electron and protons in silicon (MC4Si) and liquid water (MC4L).

MATERIALS AND METHODS

The physics

The dielectric theory in particle–solid interaction is based on the generalisation of the dielectric constant of a medium, ε , to a complex dielectric function, $\varepsilon(q, E) = \varepsilon_1(q, E) + i\varepsilon_2(q, E)$, where E and q are the energy- and momentum-transfer, respectively, to the medium. This accounts for the absorption (E -dependence) and scattering (q -dependence) properties of the medium to any sufficiently energetic external probe. In particular, the imaginary part of the inverse dielectric function

$$\text{Im} \left[\frac{-1}{\varepsilon(q, E)} \right] = \frac{\text{Im}[\varepsilon(q, E)]}{|\varepsilon(q, E)|^2} \quad (1)$$

is the key material property and is called the energy-loss-function (ELF). The numerator in Equation 1 corresponds to the single-particle spectrum of the gas phase, similar to the generalised-oscillator-strength of an atom or molecule. Condensed-phase effects are reflected in the value of the denominator. For example, for $|\varepsilon| > 1$ the long-range polarisation of the medium by the projectile's field results in a screening effect which weakens the strength of the interaction. This effect results in larger mean-free-paths in condensed matter compared with the gas-phase (when scaled to the same density). On the other hand, when $|\varepsilon| < 1$, there is an anti-screening effect, i.e. the medium strongly interacts with the particle by a collective (plasmon-like) excitation. This effect results in strong absorption peaks at about the free-electron plasmon energy of the material. In general, the effect of $|\varepsilon| \neq 1$ is to wash out the characteristic single-particle excitation peaks of the gas phase. At energy transfers, of course, much above the binding energies of the valence shells of the material, any intermolecular effects are

practically vanished and the value $|\varepsilon| \approx 1$, characteristic of the gas phase, is approached. At this range standard atomic or molecular cross-section models may be used⁽²¹⁾.

The central role of the ELF comes out from the first-Born-approximation and its expression for the doubly-differential cross-section in energy- and momentum-transfer:

$$\frac{d^2\Sigma(T, q, E)}{dq dE} = \frac{1}{\pi\alpha_0 Tq} \text{Im} \left[\frac{-1}{\varepsilon(q, E)} \right]. \quad (2)$$

It directly follows from Equation 2 that the most important transport parameters are associated with the following integrals of the ELF:

$$M^{(n)}(T) = \frac{1}{\pi\alpha_0 T} \int E^n dE \int \frac{1}{q} \text{Im} \left[\frac{-1}{\varepsilon(q, E)} \right] dq, \quad (3)$$

where for $n = 0, 1, 2$, the inelastic mean-free-path, the electronic stopping-power and the straggling parameter, respectively, are obtained.

In MC4, the ELF is determined by a two-step process: First, we establish an analytic model of the optical limit of ELF, i.e. at zero momentum-transfer ($q \approx 0$). This is the case of almost zero angular deflection which occurs at soft (or glancing) collisions. The model is based on experimental data of the optical constants, i.e. the refraction index, n , and the extinction coefficient, k , which relate to the ELF by the following relationship:

$$\text{Im} \left[\frac{-1}{\varepsilon(0, E)} \right] = \frac{2nk}{(n^2 - k^2)^2 + (2nk)^2}, \quad (4)$$

where $n = n(E)$ and $k = k(E)$ are available for both liquid water and silicon (and many other materials). In practice, the values of the optical constants are only determined for low and moderate values of E (from threshold up to a few hundred electronvolts). For higher energies the ELF may be determined from:

$$\text{Im} \left[\frac{-1}{\varepsilon(0, E)} \right] = c \frac{\mu}{\omega} \quad (5)$$

where c is the velocity of light, $\omega = \hbar/E$, and μ is the linear absorption coefficient for the photon (X ray) field. The analytic representation of the data is based on a linear combination of modified Drude functions:

$$D(E) = \sum_j \frac{f_j \gamma_j E}{(E_j^2 - E^2)^2 + (\gamma_j E)^2}, \quad (6)$$

where the E_j , f_j and γ_j are the characteristic energies, oscillator-strengths and damping coefficients, respectively. They are all treated as adjustable model parameters obtained by the fitting which

should account also for various theoretical constraints. The details of this procedure, which is quite involved, may be found elsewhere^(14, 19).

The second step involves the incorporation of the momentum-transfer dependence of the ELF by means of a dispersion model:

$$\text{Im} \left[\frac{-1}{\varepsilon(q=0, E)} \right] \xrightarrow{\text{dispersion}} \text{Im} \left[\frac{-1}{\varepsilon(q>0, E)} \right]. \quad (7)$$

This is the case where the particle transfers both energy and momentum (i.e. is deflected) to the target; the so-called hard collisions belong to this category. In the limit $E = q^2/2m$ the interaction becomes a binary, Rutherford-type, collision and, therefore, the dispersion model has to satisfy the limit:

$$\lim_{q \rightarrow \infty} \text{Im} \left[\frac{-1}{\varepsilon(q, E)} \right] \approx \delta(E - q^2/2m). \quad (8)$$

The use of a Drude optical model is particularly convenient for this task. In MC4 the q -dependence is introduced directly into the model parameters:

$$D(q, E) = \sum_j \frac{f_j(q) \gamma_j E}{(E_j^2(q) - E^2)^2 + (\gamma_j E)^2}, \quad (9)$$

where

$$E_j(q) = E_j + q^2/2m \quad (10)$$

and $f(q)$ an empirical dispersion for the oscillator strength (if available). Equation 10 is the so-called impulse approximation which directly leads to the condition of Equation 8. Alternative dispersion schemes have been examined in detail elsewhere⁽¹⁶⁾.

So far the discussion pertains to both electrons and ions. Differences between the two arise with respect to angular deflections (ions do not appreciably deflect at the present energy range), as well as, to corrections to the first-Born-approximation at very low electron energies⁽¹⁸⁾. In principle, the dielectric theory may be used to model the scattering angle in inelastic collisions, since there is one-to-one correspondence between q and θ . However, given that, in most cases, inelastic events result in $E \gg 0$ and $q \approx 0$, whereas elastic events result in $E \approx 0$ and $q \gg 0$, it is computationally advantageous to limit the use of the dielectric theory to energy-transfers only and model the scattering angles by simpler schemes. Thus, in MC4, atomic calculations or experimental datasets have been used for the angular deflections^(18,19).

The simulation

For many applications it is impractical to follow in full detail electrons above several kilo-electron-volts (often >10 – 20 keV) since, owing to the large number of interactions, computer time increases rapidly with

energy. Therefore, the transport algorithm implemented in MC4 for simulating electron trajectories uses a hybrid scheme where both a discrete (event-by-event) and a continuous (step-wise) mode of energy dissipation is being employed. The discrete scheme follows the standard procedure where a series of random numbers determine (1) the path length between successive collisions (elastic or inelastic) based on the total cross-section weighted by the exponential distribution of a Poisson stochastic process; (2) the type of collision based on the relative magnitude of the appropriate partial cross-sections and (3) the energy transfer and/or scattering angle(s) of the resultant particles based on the differential cross-sections. For inelastic events, for water, we consider five excitation transitions and five ionisation shells, whereas for silicon we consider plasmon excitation and the two inner-shells. Auger electrons out of the K-shell (and L-shell for silicon) are also accounted for. Electrons are followed down to 1 Ry (=13.6 eV) for water and 30 eV for silicon. The higher cut-off for silicon is because of the plasmon peak. The adoption of these cut-offs should not introduce any uncertainties for volumes larger than a few nanometre; this is acceptable considering other localisation uncertainties at this scale.

For electrons with energies above 10–20 keV, MC4 adopts a condensed-history random-walk scheme. That is, elastic collisions are still individually simulated (according to their cross-sections), whereas, energy dissipations by inelastic collisions in-between elastic events is considered continuous and equal to the product of the stopping-power and the chosen path length; $\Delta E = \lambda_{\text{elastic}} \times dE/dx$. The energy ΔE is assumed to be deposited randomly within the path length λ_{elastic} . Although straggling is neglected in this scheme, the simulation of individual elastic events will, for the most part, preserve the stochastics of angular deflection and, consequently, the spread-out pattern of the track. Based on this hybrid scheme, MC4 is capable of performing full slowing-down simulation of electrons of initial energy as high as 1 MeV. For protons and light ions (using the Z_{eff} -scaling) most applications consider radial distributions within track-segments. Thus, although the code extends from 100 down to ~ 0.3 – 0.5 MeV amu^{-1} , for the results presented here it was only necessary to simulate proton energy-loss within one mean-free-path (secondaries are always being followed down to cut-off). To obtain reasonable statistics, simulations have been performed for 10,000 electron histories and 50,000 proton histories.

RESULTS

In Figure 1a and b, the radial distribution of energy deposition (not dose) by electrons and protons is depicted for the two materials examined. For

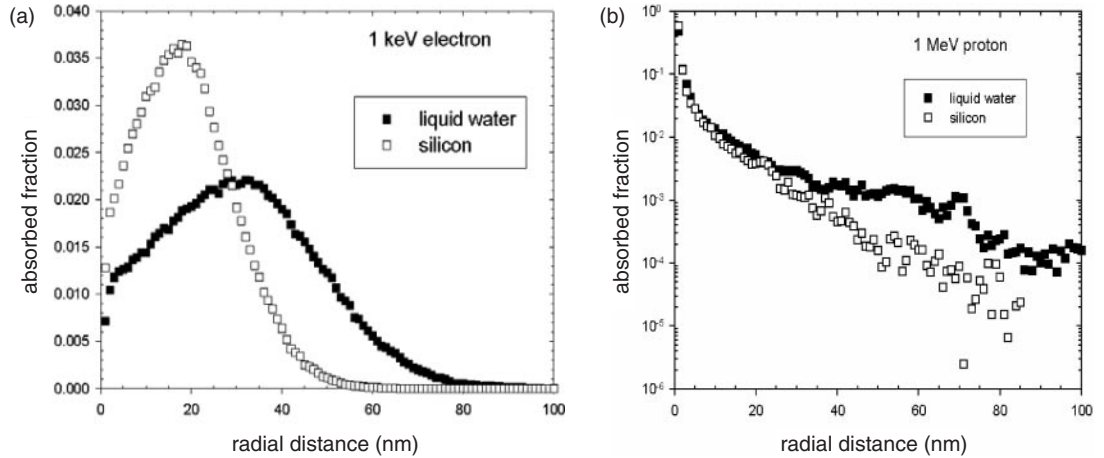


Figure 1. Normalised absorbed energy distributions: (a) Spherical distribution around the origin of electron tracks (normalisation to the incident electron energy); (b) Cylindrical distribution around the axis of proton track-segments (normalisation to the proton energy-loss).

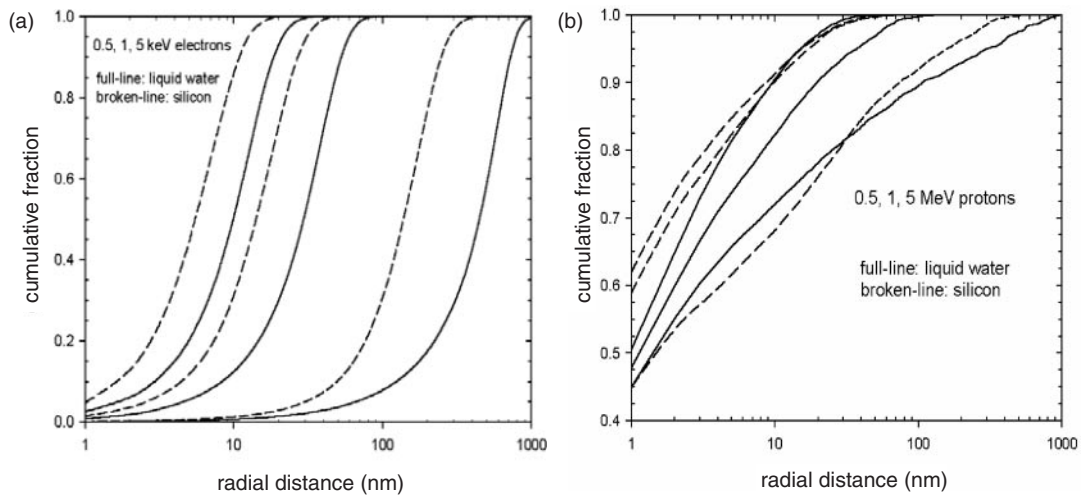


Figure 2. Cumulative distributions of absorbed energy: (a) spherical distribution around the origin of electron tracks; (b) cylindrical distribution around the axis of proton track-segments.

electrons (Figure 1a) a spherical geometry has been used, i.e. the radial distance denotes spherical shells around the point of origin of the primary electron. The absorbed energy is normalised to the initial electron energy. The results have been obtained by following both the primary and secondary electrons until complete stopping. In contrast, for protons (Figure 1b) a cylindrical geometry has been used around the axis of a proton track-segment. The absorbed energy has been normalised to the proton energy-loss along the track-segment. Practically, protons are followed until only their first collision,

whereas secondary electrons until they stop. Both figures reveal the effect of the strong plasmon excitation which exists in silicon. Since most secondaries originate with energies up to a few tens of electron volts where the plasmon cross-section (the L- and K-shells do not contribute) in silicon is larger by a factor of 2 (or more) than the total inelastic cross-section in water, the diffusion of low-energy secondaries in silicon is restricted very close to their point of origin (small mean-free-paths) resulting in the rapid dissipation of their energy. From Figure 2a and b, it may be seen that the above effect persists

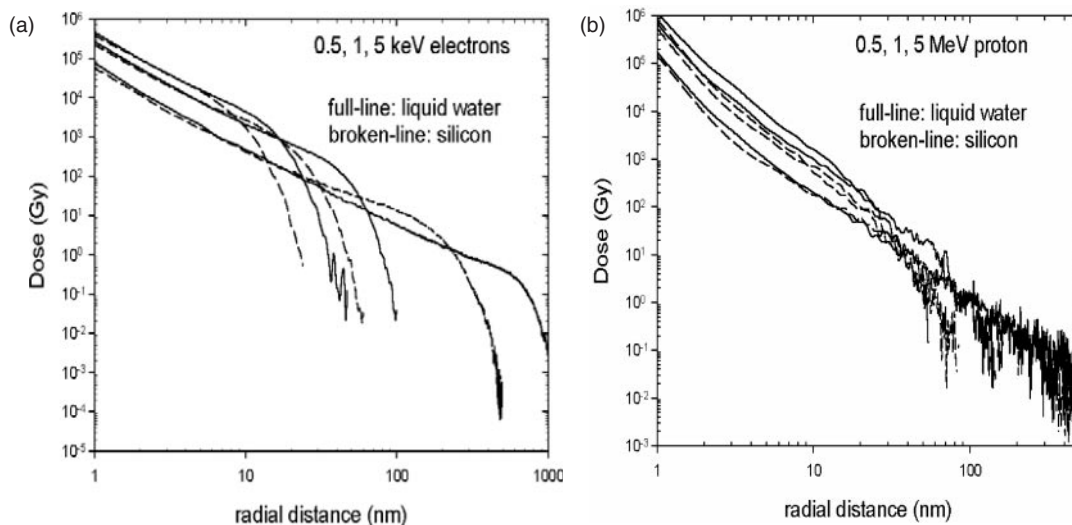


Figure 3. Radial dose profiles: (a) spherical distribution around the origin of electron tracks; (b) cylindrical distribution around the axis of proton track-segments.

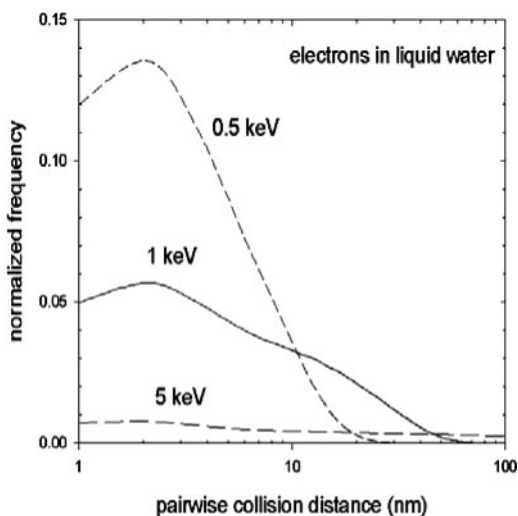


Figure 4. Probability distribution of separation distance of two energy deposition events within an electron track in liquid water.

at all incident energies and, in general, tracks in silicon have a smaller spread-out pattern. Such results may also be used in modelling phase transformation and latent track formation in solid detectors by calculating energy deposition within sub-micron regions around the track.

An important quantity for various microscopic calculations is the radial dose distribution. Such results are depicted in Figure 3a and b for electrons

(spherical geometry) and protons (cylindrical geometry) in the two materials. For example, the radially-restricted LET, which is an important quantity not easily amenable to an analytic calculation, may be directly found by such data. As we have shown elsewhere, fitting formula could be used to analytically represent the radial distribution of dose for both types of charged particles. It has been found that the exact r -dependence for protons is much more involved than a simple power-like law ($\propto 1/r^n$), while for both particles the dose decreases much faster than $1/r^2$, at least initially.

In Figure 4, as an example of a simple clustering analysis, we present the probability distribution of finding two energy deposition events at a certain distance to each other for electron tracks in liquid water. Along with a consideration on the structure of biological targets, such information provides insight for predicting effect probability. It may be seen, for example, that in a 500 eV electron track, the probability distribution peaks at 2 nm, which coincides exactly with the diameter of the DNA double helix. The peak broadens as the electron energy increases, and at a few kilo-electron-volts becomes almost flat for a substantial spatial range (1–100 nm), which covers the dimensions of most of the sub-nuclear cellular structures.

Figure 5 presents the probability distribution of electron-hole separation distances in silicon for proton track-segments. Such information is important in calculating prompt electric fields around the track, which influence the charge-carrier recombination process. Direct information on such

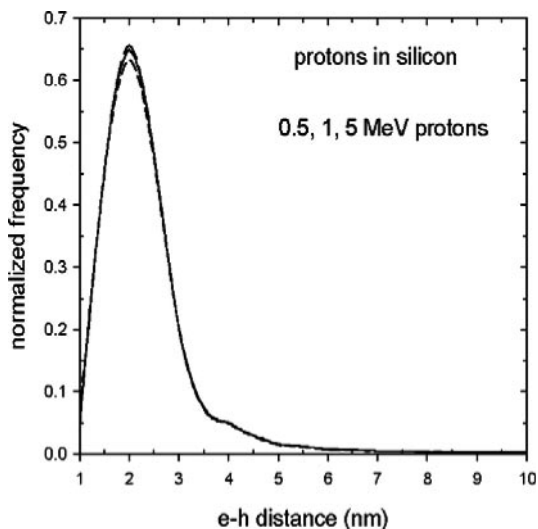


Figure 5. Probability distribution of electron-hole separation distance in proton track-segments in silicon.

effects is difficult to obtain experimentally and, therefore, such simulation results are particularly relevant.

ACKNOWLEDGEMENTS

This work was partly supported by the United Kingdom Department of Trade & Industry (DTI) (grant QCBB/013/00057), and by grant 62/1405 registered with the University of Ioannina Committee of Research.

REFERENCES

- Rossi, H. and Zaider, M. *Microdosimetry and Its Applications*. (Berlin: Springer) (1996).
- Akkerman, A. F. and Gibrekhterman, A. L. *Comparison of various Monte Carlo schemes for simulation of low-energy electron transport in matter*. Nucl. Instrum. Methods **B6**, 496–503 (1985).
- Kaplan, I. G. *The track structure in condensed matter*. Nucl. Instrum. Methods **B105**, 8–13 (1995).
- Ritchie, R. H., Hamm, R. N., Turner, J. E., Wright, H. A. and Ashley, J. C. *Physical aspects of charged particle track structure*. Nucl. Tracks Radiat. Meas. **16**, 141–155 (1989).
- Tanuma, S., Powel, C. J. and Penn, D. R. *Calculations of electron inelastic mean free paths*. Surf. Interface Anal. **21**, 165–176 (1993).
- Kwei, C. M., Chen, Y. F., Tung, C. J. and Wang, J. P. *Electron inelastic mean free paths for plasmon excitations and interband transitions*. Surf. Sci. **293**, 202–210 (1993).
- Jensen, K. O. and Walker, A. B. *Monte Carlo simulation of the transport of fast electrons and positrons in solids*. Surf. Sci. **292**, 83–97 (1993).
- Dingfelder, M., Hantke, D., Inokuti, M. and Paretzke, H. G., *Electron inelastic-scattering cross-sections in liquid water*. Radiat. Phys. Chem. **53**, 1–18 (1998).
- Akkerman, A. and Akkerman, E. *Characteristics of electron inelastic interactions in organic compounds and water over the energy range 20–10000 eV*. J. Appl. Phys. **86**, 5809–5816 (1999).
- Baro, J., Sempau, J. M., Fernandez-Varea, J. M. and Salvat, F. *PENELOPE: an algorithm for Monte Carlo simulation of the penetration and energy loss of electrons and positrons in matter*. Nucl. Instrum. Methods **B100**, 31–46 (1995).
- Fernandez-Varea, J. M., Liljequist, D., Csillag, S., Raty, R. and Salvat, F. *Monte Carlo simulation of 0.1–100 keV electron and positron transport in solids using optical data and partial wave methods*. Nucl. Instrum. Methods **B108**, 35–50 (1996).
- Ballarini, F., Biaggi, M., Merzagora, M., Ottolenghi, A., Dingfelder, M., Friedland, W., Jacob, P. and Paretzke, H. G. *Stochastic aspects and uncertainties in the prechemical and chemical stages of electron tracks in liquid water: a quantitative analysis based on Monte Carlo simulations*. Radiat. Environ. Biophys. **39**, 179–188 (2000).
- Cobut, V., Cirioni, L. and Patau, J. P. *Accurate transport simulation of electron tracks in the energy range 1 keV–4 MeV*. Nucl. Instrum. Methods **B215**, 57–68 (2004).
- Emfietzoglou, D. and Moscovitch, M. *Inelastic collision characteristics of electrons in liquid water*. Nucl. Instrum. Methods **B193**, 71–78 (2002).
- Emfietzoglou, D. and Moscovitch, M. *Secondary electron spectra for fast proton impact on gaseous and liquid water*. Nucl. Instrum. Methods **B209**, 239–245 (2003).
- Emfietzoglou, D. *Inelastic cross-sections for electron transport in liquid water: a comparison of dielectric models*. Radiat. Phys. Chem. **66**, 373–385 (2003).
- Emfietzoglou, D., Moscovitch, M. and Pathak, A. *Inelastic cross-sections of energetic protons in liquid water calculated by model dielectric functions and optical data*. Nucl. Instrum. Methods **B212**, 101–109 (2003).
- Emfietzoglou, D., Karava, K., Papamichael, G. and Moscovitch, M. *Monte-Carlo simulation of the energy-loss of low-energy electrons in liquid water*. Phys. Med. Biol. **48**, 2355–2371 (2003).
- Emfietzoglou, D., Akkerman, A. and Barak, J. *New Monte-Carlo calculations of charged particle track-structure in silicon*. IEEE Trans. Nucl. Sci. **51**, 2872–2879 (2004).
- Zaider, M., Vracko, M. G., Fung, A. Y. C. and Fry, J. L. *Electron transport in condensed water*. Radiat. Prot. Dosim. **52**, 139–146 (1994).
- Rudd, M. E., Kim, Y.-K., Madison, D. H. and Gay, T. J. *Electron production in proton collisions with atoms and molecules: energy distributions*. Rev. Mod. Phys. **64**, 441–490 (1992).